MAGNETIC DEPOSITS OF IRON OXIDES IN THE HUMAN BRAIN

MIROSLAVA MAKOHUSOVÁ,[a] VIERA MRÁZOVÁ,[a]
MARTIN KOPÁNI,[b] ROMAN BOČA[a]

[a]*Department of Chemistry, University of SS. Cyril and Methodius in Trnava, SK-917 01 Trnava, Slovakia (roman.boca@stuba.sk)*
[b]*Institute of Medical Physics, Biophysics, Informatics and Telemedicine, Faculty of Medicine, Comenius University, Bratislava, Slovakia*

Abstract: Deposits of iron oxides in the human brain (*globus pallidus*) are visible under electron microscopy as object of regular and or/irregular shape but giving sharp diffraction patterns in the transmission mode. The SQUID magnetometry reveals that the magnetization curves decline form an ideal Langevin function due to the dominating diamagnetism of organic tissue. The fitting procedure yields the quantitative characteristics of the overall magnetization curves that were further processed by statistical multivariate methods.

Key words: human brain, electron microscopy, iron oxides, hematite, magnetite, maghemite, SQUID magnetometry

1. Introduction

Several studies confirm that iron oxides appear as mineral deposits in various areas of the human brain (KIRSCHVINK *et al*., 1992). The deposits differ in the size (typically from 10 – 50 nm) and composition given by the content of Fe(III) and Fe(II). These deposits differ from the ferritin inorganic core (6 nm in size) in many physical characteristics. The ferritin (e.g. the horse spleen ferritin, as a reference) is an iron storage protein containing *ca* 4500 atoms of Fe(III) in the form of the ferrihydrite and magnetically it behaves as a paramagnet until T_c = 16 K. Below this critical temperature it behaves as a superparamagnet that possesses the out-of-phase (imaginary) susceptibility component measured in the AC (alternating current) mode. Moreover it exhibits a magnetic hysteresis which, however, escapes above T_c so that it is absent at the room temperature. [Ferrihydrite is hexagonal with the unit cell parameters a = 2.96 and c = 9.4 Å, but variable water content formulated as $5Fe_2O_3{\cdot}9H_2O$, $Fe_5HO_8{\cdot}4H_2O$, $Fe_5O_3(OH)_9$, $Fe_2O_3{\cdot}2FeOOH{\cdot}2.6H_2O$, $FeOOH{\cdot}0.4H_2O$, and also $Fe_2O_3{\cdot}0.5H_2O$.]

In the previous work (KIRSCHVINK *et al*., 1992) the deposits of iron oxides in *Cerebellum* were identified as nanocrystals of magnetite, Fe_3O_4 ($Fe^{II}O{\cdot}Fe^{III}{}_2O_3$), possessing the cubic unit cell. This mineral is a ferrimagnet at the room temperature. Another magnetic mineral is maghemite, γ-Fe_2O_3, that again possesses the cubic unit cell with the structure derived from magnetite with Fe(II) deficient vacancies. Maghemite nanoparticles are non-toxic and biocompatible so that they found application in biomedicine through their manipulation with external magnetic field (PANKHURST *et al*., 2003; GUBIN *et al*., 2009).

DOI 10.2478/nbec-2014-0006

Single crystals of hematite, α-Fe_2O_3, have been detected recently in *basal ganglia* (region *globus pallidus*) by means of the TEM mode of the electron microscopy (BOČA *et al*., 2013). Hematite possesses the hexagonal unit cell. In bulk it is an antiferromagnetic material below T_c = 250 K and a canted antiferromagnet (weak ferromagnet) above this (Morin) temperature; above the Néel temperature T_N = 948 K it behaves as a paramagnet. In the other words, bulk hematite is non-magnetic at the room temperature. Hematite nanoparticles have different magnetic properties when compared to bulk as with lowering the particle size the Morin transition decreases. Notice, hematite is the most stable iron oxide from the point of view of thermodynamics.

2. Experimental section

Samples from the human brain were extracted post mortem at the authorized department in accordance with Helsinki Declaration (only the age and gender of the donors is available).

Fresh samples were fixed in 10 % formaldehyde for 24 hours and embedded in paraffin blocks, cut by microtome to 5 μm thin sections and mounted on gelatin-coated slides. Samples without cover glass were analysed by scanning electron microscope (JXA 840 A, JEOL) with the accelerating voltage of 20 kV. The samples for transmission electron microscopy were fixed in 3% solution of glutar(di)aldehyde (SERVA, Heidelberg) for two hours and buffered by phosphate (pH 7.2 – 7.4), embedded into Durcupan ACM (Fluka AG, Busch) as recommended by the manufacturer and cut by ultramicrotome (C. Reichert, Vienna) to the thickness of 200 nm. Noncontrasted ultrathin sections were mounted on nickel grids and investigated by transmission electron microscope with acceleration voltage of 120 kV.

Fresh tissues were lyophilized and the resulting samples were obtained in a form of a powder. Attention was paid to avoid manipulations with magnetisable instruments and environment. The Superconducting Quantum Interference Device (SQUID, Quantum Design, MPMS-XL7) has been used for measurements of the magnetic moment of the sample in the sensitive RSO mode. Powder samples were encapsulated into gelatin-made sample holders. Magnetization measurements were performed at T = 2.0 and 4.6 K, respectively, in the field-decreasing mode starting from B = 7.0 T. The susceptibility measurements between 2 and 300 K were done at the small applied field of B = 0.1 T.

3. Results and discussion

Photographs of the hematite deposits found in *globus pallidus* are presented in Fig. 1. Miller indices in the TEM mode unambiguously confirm the hexagonal unit cell characteristic for the hematite. This finding is in contrast with the generally accepted statement (CORNELL *et al*., 2003): "With the exception of hematite, all the major oxides are found in living organisms. The absence of hematite suggests that biological environments do not provide suitable conditions for the formation of this oxide." Unexpected is also the size of the deposits that exceeds 1000 nm.

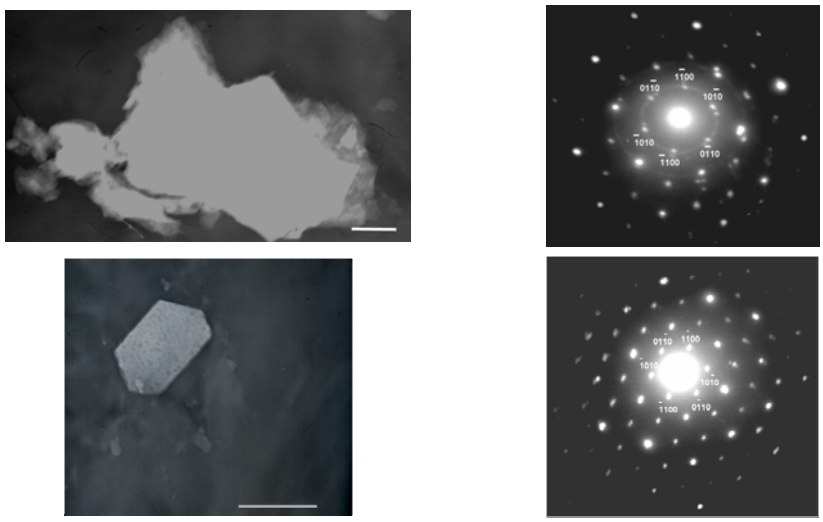

Fig. 1. Hematite deposits in the human brain of irregular and regular shape along with TEM diffractograms. Marker – 1000 nm.

Temperature evolution of the magnetic susceptibility of 16 samples is presented in the form of a product function χT in Fig. 2. Deviation from the straight line with zero slope means that the Curie law is not obeyed. Class I is represented by 9 samples exhibiting a dominating diamagnetic signal for which the χT product decreases with increasing temperature. Class III contains 3 samples showing the positive magnetic susceptibility in the whole temperature region and consequently the χT product function possesses a positive slope. Class-II covers 4 samples that are intermediate between class-I and class-III.

The magnetization curves for the samples under study are presented in Fig. 3. These records arise from the combination of the classical magnetization curve according to the Langevin function $L(x) = [\coth(x) - 1/x]$ and a superimposed diamagnetic background (χ_{dia}) owing to the organic tissue

$$M_{mass}(B,T) = w_{PF} \cdot M_{para} + (1 - w_{PF}) \cdot (\chi_{dia} / \mu_0) B_{ext} \quad (1)$$

with

$$M_{para} = M_{Fe} \cdot (N_A \mu_B \mu) \cdot [\coth(x) - 1/x] \quad (2)$$

for the argument

$$x = \mu_B \mu (B_{ext} + B_{int}) / k_B T \quad (3)$$

Here μ – magnetic moment in units of Bohr magneton, M_{Fe} – the molar mass of iron, w_{PF} – mass fraction of the paramagnetic species, and physical constants adopt their usual meaning. The internal magnetic field is parameterized by the Weiss field constant (W) as $B_{int} = W \cdot M$ and causes the existence of the remnant magnetization and consequently the magnetic hysteresis. The above equations need be solved by an iterative procedure.

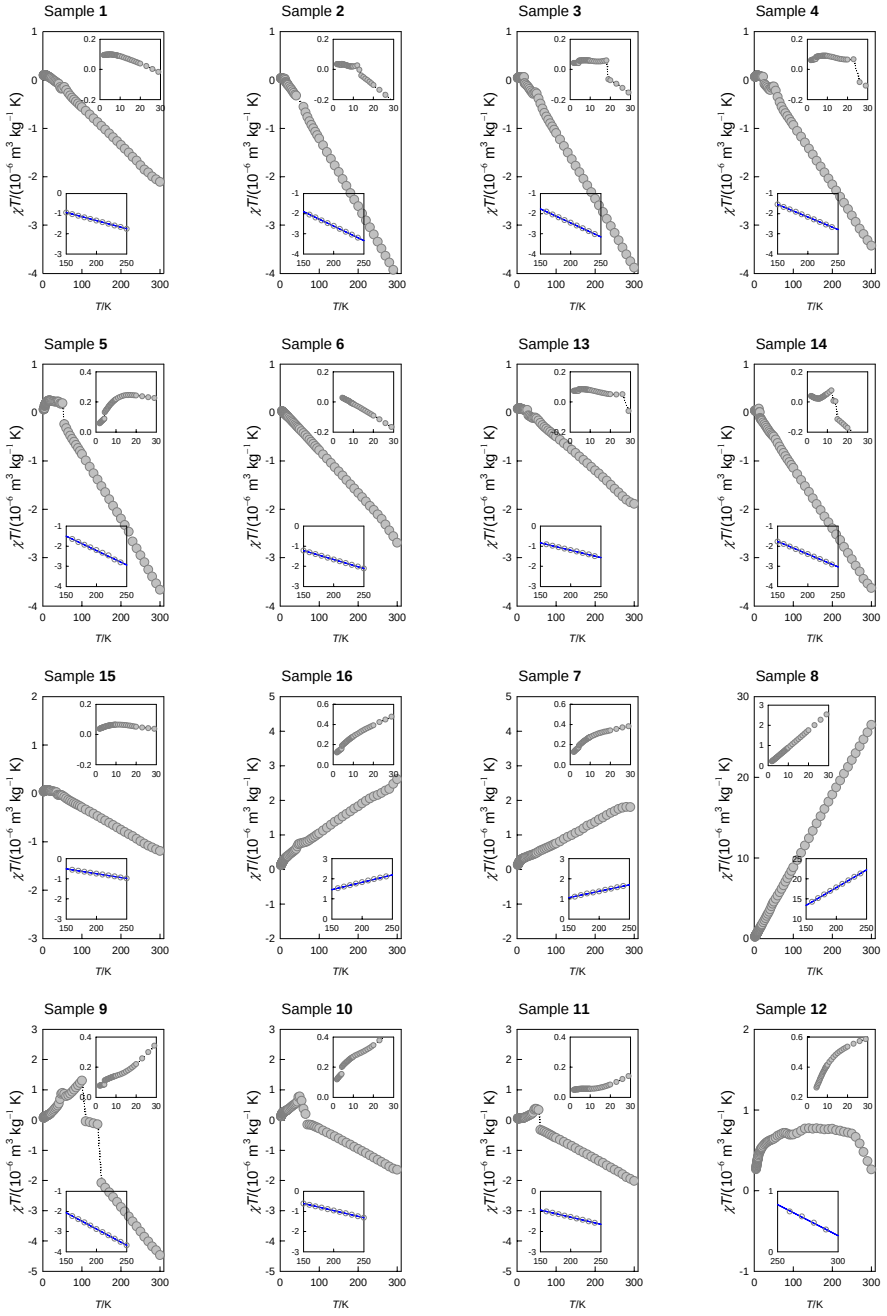

Fig. 2. Mass magnetic susceptibility in form of the product function χT *vs* T and its high-temperature fit.

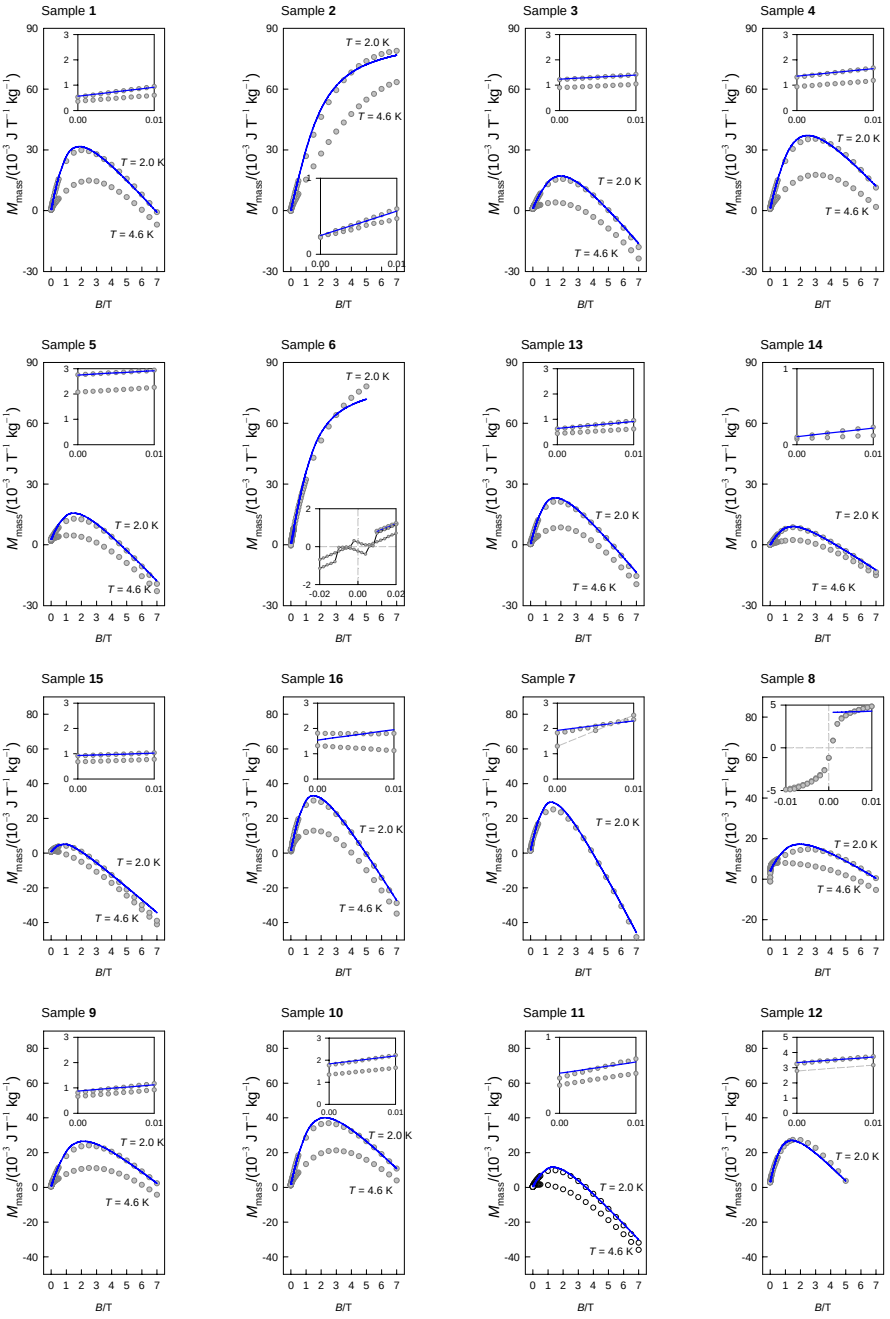

Fig. 3. Mass magnetization and its fit for $T = 2.0$ K (solid line) with the modified Langevin function.

The fitting procedure applied to data referring to $T = 2.0$ gave the parameters that are listed in Table 1. A great win is that in prevailing cases the model describes correctly the magnetization curves including the remnant magnetization. As a result, four variables were determined: the mass fraction of the paramagnetic species (w_{PF}), diamagnetic background (χ_{dia}), mean magnetic moment (μ), and the Weiss-field constant (W).

Also the χT product function in the interval $T = 150 – 250$ K has been fitted by a straight line $\chi T = C + \alpha T$ and the data are presented in Table 1.

The data shows that the mass fraction of the magnetic iron in the lyophilized samples under study is of the order of 10^{-4}. The observed paramagnetic contribution is due to the minor fraction of paramagnetic metals (Cu^{2+}, Fe^{2+} in hemoglobin), ferritin, and dioxygen molecules; the ferromagnetic contribution arises from the strong signal of γ-Fe_2O_3 and Fe_3O_4 deposits, respectively. Nanoparticles of α-Fe_2O_3 could also contribute through the uncompensated magnetic moments of the surface atoms.

Table 1. Parameters of the susceptibility and magnetization for samples under study. [a]

Sample	Class	Age	C	α / 10^{-3}	w_{PF} /10^{-6}	Background (χ_{dia}/μ_0)×10^{-3}	μ/μ_B	W / 10^{-3}	Remanence M_R / 10^{-3}	
									2.0 K	4.6 K
	Abbr.	age	C	a	wPF	dia	m	FW	RM2	RM4
1	I	52	0.27	-8.1	106.0	-8.74	6.03	0.41	0.52	0.35
2	I	61	0.25	-14.3	267.4	0	3.25	0.48	0.22	0.23
3	I	65	0.31	-13.9	127.6	-9.25	4.17	2.35	1.21	0.90
4	I	69	0.34	-12.5	190.5	-8.76	4.22	1.66	1.31	0.93
5	I	85	0.64	-14.3	79.4	-8.13	5.26	4.08	2.75	2.24
6 w	I	69	0.11	-8.9	190.0	0	4.32	0.47	0.24	0.24
7	III	53	0.099	6.4	127.6	-17.14	6.14	1.10	1.82	1.29
8	III	58	0.23	87.8	81.8	-4.90	4.59	9.09	0	0
9	II	38	0.34	-16.1	120.1	-7.36	4.83	1.12	0.80	0.66
10	II	66	0.44	-7.0	162.7	-9.22	4.98	1.57	1.76	1.34
11	II	76	0.14	-7.1	70.4	-9.51	5.51	0.76	0.46	0.37
12 w	II	83	3.33	-10.2	72.0	-9.38	7.51	1.87	3.24	2.78
13	I	40	0.27	-7.3	89.2	-9.15	5.99	0.57	0.61	0.44
14	I	60	0.12	-12.6	41.8	-5.09	5.88	0.21	0.097	0.072
15	I	64	0.19	-4.7	24.3	-7.52	7.86	1.31	0.91	0.68
16	III	73	0.35	7.2	122.4	-14.4	6.32	0.84	1.81	1.31

[a] Curie constant C in $m^3\ kg^{-1}\ K$ [SI], temperature-independent susceptibility (TIS) α in $m^3\ kg^{-1}$ [SI], remnant magnetization M_R in $J\ T^{-1}\ kg^{-1}$ [SI], mass fraction of the paramagnetic fraction w_{PF} – dimensionless, Weiss field W in [SI], magnetic moment μ in Bohr magnetons μ_B, background diamagnetism (χ_{dia}/μ_0) in [SI]. w - women.

The quantitative characteristics of the fitted magnetization and susceptibility were processed by statistical multivariate methods: Correlation (C), Cluster analysis (CA), Principal component analysis (PCA), and Factor analysis (FA) dealing with 9 variables (*age*, *C*, *a*, *wPF*, *dia*, *m*, *FW*, *RM2* and *RM4*).

With exception of samples No 8 and 12, the CA shows three mostly separated clusters containing 6, 6, and 2 members, respectively, according to their similarity (squared Euclidean distance) – Fig. 4. Sample No 8 resembles features of a

metamagnet and possesses some characteristics (α, W) unlike to the others; therefore this sample was deleted from further statistical processing. Also the sample No 2 is very different from the others (see Fig. 2). After this omission, the samples are a bit rearranged into two distant clusters as seen from Fig. 4 – right.

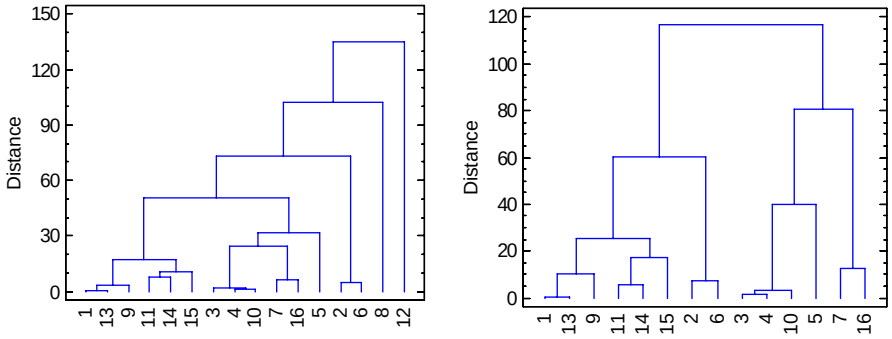

Fig. 4. Dendogram of the Cluster Analysis (Wards method, metric – squared Euclidean). Left – all data, right – selected data.

The PCA generates a new set of variables through a linear combination of the original set (Fig. 5). New components bear maximum information about the variability of data. The two principal components account 73 % of the variance in the data (43.6 and 29.4 %, respectively). Lines are used to reflect the variables of the dataset, and circles show the observations. The biplot in Figure 5 separates variables into three groups according to their strong interrelations: 1 – {*age*, *C*, *FW*, *RM4*, *RM2*}, 2 – {*m*, *a*}, and 3 – {*dia*, *wPF*}. The relationship between group 1 and group 2, and between group 1 and group 3 is weak. The correlation between group 2 and group 3 is strong-negative. The length of the lines approximates the variances of the variables, the longer the line, the higher is the variance.

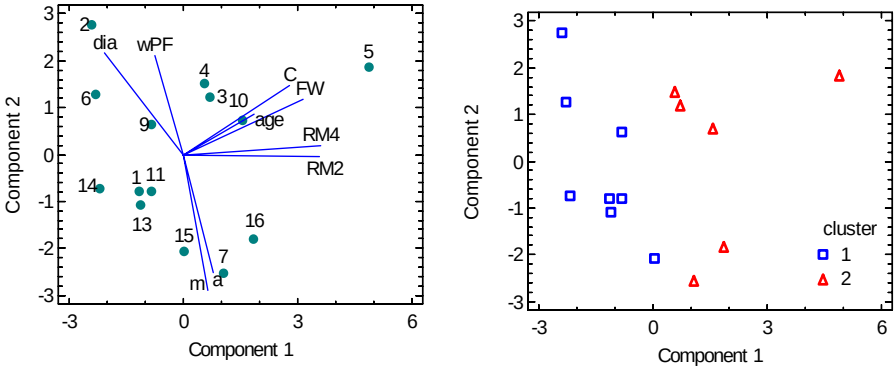

Fig. 5. Biplot according to the Principal Component Analysis.

The samples 5, 10, 3, 4, 16 and 7 (forming the cluster No 1) have higher values of the variables from the group 1. The sample 2 has the highest value of *dia* and *wPF*, the

samples 15, 7 and 16 has the high values of *m* and *a*. Points that are close together correspond to observations that have similar values of the variables.

The FA reconstructs the original variables from a new, fictitious set with the same aim as PCA (Fig 6, after varimax rotation). It is seen that the variables {*age*, *C*, *FW*, *RM4*, *RM2*} are closely related whereas other groups are formed by {*m*, *a*} and {*dia*, *wPF*} variables.

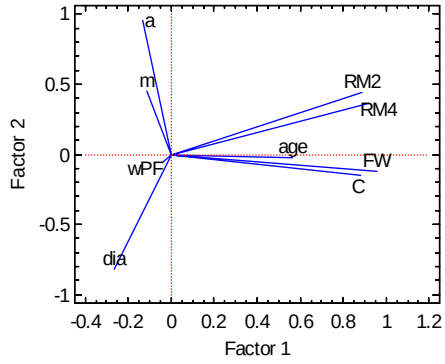

Fig. 6. Biplot according to the Factor Analysis.

The correlation coefficients between pairs of variables are listed in Table 2. Two remnant magnetizations (*RM2* and *RM4*) are strongly interrelated, as expected: r = 0.99. They correlate with the Weiss field constant (*FW*), $r > 0.80$, and also with the susceptibility parameter (*C*), $r > 0.70$. The last variable adopts function of the Curie constant in the formula $\chi = C/T + \alpha$ whereas α is the temperature-independent term reflecting either the diamagnetism of the organic tissue ($\alpha < 0$, in class-I and II) and/or ferromagnetism ($\alpha >> 0$, in class-III). *RM2* also negatively correlates with diamagnetic background *dia*. Temperature-independent susceptibility *a* is positively correlated with mean magnetic moment *m*, and negatively correlated with diamagnetic background *dia*. The mass fraction of the paramagnetic species *wPF* negatively correlates with the mean magnetic moment *m*. These results are in agreement with those from the PCA.

Table 2. Correlation coefficients using 14 datapoints [a]

	age	C	a	wPF	dia	m	FW	RM2
C	0.3083							
a	0.0459	-0.2848						
wPF	0.0120	0.0631	-0.1539					
dia	0.0450	-0.1106	*-0.6939*	0.3670				
m	-0.0947	-0.1833	*0.5795*	*-0.8134*	-0.5052			
FW	0.5031	*0.7783*	-0.2480	-0.1178	-0.1981	-0.1078		
RM2	0.4194	*0.7143*	0.2982	-0.0799	*-0.6052*	0.1330	*0.8029*	
RM4	0.4484	*0.7528*	0.2275	-0.0726	-0.5323	0.0933	*0.8407*	*0.9942*

[a] Colored (Italic) cells indicate statistically significant correlations at the 95.0% confidence level.

The Correlation Analysis reveals that the age of the donors (weakly) correlates with variables that characterize ferromagnetism of iron-oxide deposits. Such correlations are visualized by plots in Fig. 7.

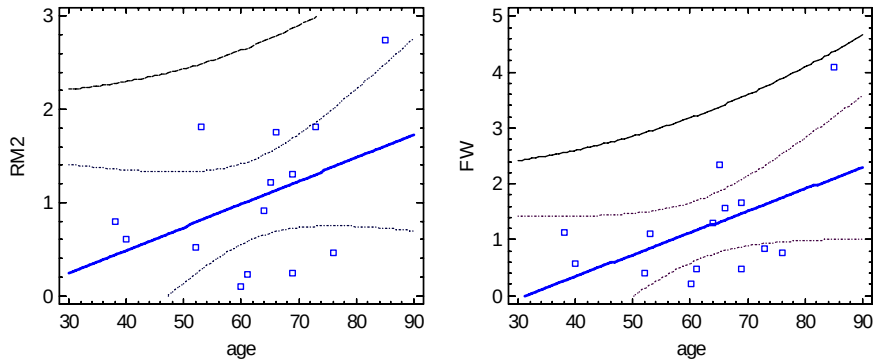

Fig. 7. Linear correlations of characteristics of the magnetic deposits with age of the donors: left – remnant magnetization *RM2* = –0.51 + 0.025**age*, Weiss field *FW* = -1.22 + 0.030**age*. Confidence and prediction intervals are shown at 95 % probability level.

4. Conclusions

It has been demonstrated that in basal ganglia of the human brain some deposits of iron oxides are accumulated. Microcrystals of hematite were detected by the electron microscopy (TEM). The SQUID magnetometry reflects diamagnetism of the organic tissue, non-magnetic deposits like hematite, paramagnetic centers including ferritin, and ferro(ferri) magnetic deposits as maghemite. It was found that the individual characteristics of the diamagnetism (*a*, *dia*), paramagnetism (*C*, *wPF*), and ferro(ferri)magnetism (*FW*, *RM2*, *RM4*) are mutually interrelated. The most important finding is that the content of the magnetic deposits (*wPF*) does not correlate with the age of the donors. However, the parameters of the ferro(ferri)magnetism *FW* and *RM2* (*RM4*) correlate with the age: on aging of the donors the ferromagnetic productivity of the deposits increases.

Acknowledgements: Slovak grant agencies (VEGA 1/0233/12, VEGA 1/0220/12 and APVV-0014-11) are acknowledged for the financial support.

References

BOČA, R., KOPÁNI, M., MIGLIERINI, M., ČAPLOVIČOVÁ, M., MRÁZOVÁ, V., DLHÁŇ, Ľ.: Magnetic and Non-Magnetic Iron-Oxide Deposits in Basal Ganglia. *In* COSTA, A., VILLALBA, E. (Eds.), Volume 12: Horizons in Neuroscience Research. Nova Science Publishers, Inc., New York, 2013, 135-214.

CORNEL, R. M., SCHWERTMANN, U.: The Iron Oxides: Structure, Properties, Reactions, Occurrences and Uses, Wiley-VCH, Weinheim, 2003, 703 pp.

GUBIN, S. P. (Ed.): Magnetic Nanoparticles, Wiley-VCH, Weinheim, 2009.

KIRSCHVINK, J. L., KOBAYASHI-KIRSCHVINK, A., WOODFORD, B. J.: Magnetite biomineralization in the human brain. Proc. Natl. Acad. Sci. USA, 89, 1992, 7683-7687.

PANKHURST, Q. A., CONNOLLY, J., JONES, S. K., DOBSON, J.: Applications of magnetic nanoparticles in biomedicine. J. Phys. D: Appl. Phys., 36, 2003, 167-181.